RSC Advances

PAPER

View Article Online
View Journal | View Issue

Cite this: *RSC Adv.*, 2017, **7**, 29883

Investigation of myrrh extract as a new corrosion inhibitor for α-brass in 3.5% NaCl solution polluted by 16 ppm sulfide

H. S. Gadow, *[a] M. M. Motawea[b] and H. M. Elabbasy[c]

This study investigates the performance of myrrh plant extract as a corrosion inhibitor for a copper–zinc alloy in 3.5 wt% NaCl solution polluted by 16 ppm sulfide. The inhibition behavior was determined through a gravimetric method, electrochemical measurements, AFM, UV spectroscopy and FTIR. The results demonstrated that the efficiency of inhibition increases with increasing concentration of the myrrh extract and decreases with temperature. The corrosion rate of a copper –zinc alloy was decreased in the presence of myrrh extract. The corrosion inhibition efficiency was found to increase with myrrh concentration to a value of 67% at 300 ppm and 25 °C. The thermodynamic activation parameters that govern the process were deduced from the temperature dependence. Potentiodynamic polarization curves indicated that the myrrh extract behaves as a mixed-type inhibitor. This extract was adsorbed on a copper alloy surface following the Langmuir adsorption isotherm and a kinetic model adsorption isotherm. The adsorption free energy of the myrrh extract on the copper zinc alloy reveals a physical adsorption of myrrh on the alloy surface. The results of atomic force microscopy, and Fourier transform infrared and UV-visible spectrophotometric methods support the electrochemical measurements and gravimetric method.

Received 15th April 2017
Accepted 25th May 2017

DOI: 10.1039/c7ra04271j

rsc.li/rsc-advances

1. Introduction

Corrosion of copper and its alloys has attracted much attention from many researchers because copper and its alloys have a wide variety of applications in industry and technology which we use extensively in many types of chemical equipment including pumps, valves, evaporators, fans and fractionating columns. Large quantities of pipes made out of copper and copper alloys are used to make heat exchangers and condensers, where fresh or salt water is used for cooling. Use in all of these applications is because copper and its alloys have thermal and electrical conductivity, and also they have good mechanical workability, low cost and excellent resistance to corrosion in neutral aggressive media. For this reason and because electrodissolution of copper in chloride solutions is important in electropolishing and electromachining, there is an interest in inhibitors that can be used in marine environments.[1–5] The pollution of seawater with sulfide in coastal areas can occur due to bacteriological and biological processes taking place in seawater and also because of industrial waste water discharge into the sea. Thus, corrosion of copper alloys in seawater polluted with sulfide ions is a serious problem.

Alloys of copper have sufficient resistance to corrosion in seawater. However, they corrode under special conditions. The anodic dissolution mechanism of brass in neutral chloride media can be demonstrated as follows: in the first stage of corrosion, a ZnO layer is formed on the brass surface *via* the reaction:

$$Zn^{2+} + H_2O \rightarrow ZnO + 2H^+$$

or

$$Zn + 4Cl^- \rightarrow ZnCl_4^{2-} + 2e^-$$

In the presence of chloride, cuprous ions are stable, and this species forms CuCl, which will then be transformed into $CuCl_2^-$ ions.[6,7]

$$Cu + 2Cl^- \rightarrow CuCl_2^- + e^-$$

The presence of $CuCl_2^-$ at the metal surface leads to the formation of Cu_2O[8]

$$2CuCl_2^- + H_2O \rightarrow Cu_2O + 4Cl^- + 2H^+$$

Sulfide is considered as the common pollutant which causes intensive corrosion of copper alloys in seawater where

[a]Higher Institute for Engineering and Technology, New Damietta, Egypt. E-mail: ahsgado73@gmail.com
[b]Delta Higher Institute for Engineering and Technology, Mansoura, Egypt
[c]Misr Higher Institute for Engineering and Technology, Mansoura, Egypt

the presence of sulfide ions leads to the modification of the oxide layer on copper based alloys and acceleration of corrosion is due to the enhancement of the cathodic process. From the important parameters playing a major part in the processes of corrosion of copper alloys in seawater polluted with sulfides, one of the most important is their concentration.[9,10] The corrosion mechanism of copper in sulfide containing medium will be presented by the following equations:[11,12]

$$O_2 + 2H_2O + 4e^- \leftrightarrow 4OH^-$$

In the presence of sulfide, HS^- will be formed:

$$S^{2-} + H_2O \leftrightarrow HS^- + OH^-$$

Combination of HS^- with copper:

$$Cu + HS^- \rightarrow Cu(HS^-)_{ads}$$

Anodic dissolution of copper:

$$Cu(HS^-) \rightarrow Cu(HS) + e^-$$

Finally, dissociation and recombination processes:

$$Cu(HS) \rightarrow Cu^+ + HS^-$$

$$2Cu^+ + HS^- + OH^- \rightarrow Cu_2S + H_2O$$

The overall reaction:

$$4Cu + 2S^{2-} + O_2 + 2H_2O \leftrightarrow 2Cu_2S + 4OH^-$$

The use of inhibitors is one of the techniques for minimizing corrosion. The effectiveness of the inhibitors varies with their concentrations, the corrosive medium and the surface properties of the alloy. Many inhibitors have been used to minimize the corrosion of brass in different media.[13–18] Natural products of plant origin are readily available, inexpensive, and eco-friendly corrosion inhibitors.[19–21] Extracts from their leaves, barks, seeds, and roots are composed of a mixture of organic compounds and some have been reported as effective inhibitors for various metals and alloys. These organic compounds usually contain polar functions with nitrogen, sulfur or oxygen atoms and have triple or conjugated double bonds with aromatic rings in their molecular structures, which are the major adsorption centers.[22,23]

The aim of this paper is to explore, for the first time, the use of myrrh extract as a corrosion inhibitor for α-brass in 3.5% NaCl solution polluted by 16 ppm sulfide.

2. Materials and methods

2.1 Materials

The chemical composition of the used α-brass (weight%) is Cu 67.28, Pb 0.029, Fe 0.002 and Zn 32.689. First, the samples were mechanically cut and prepared into five pieces each of dimensions 20 × 20 × 1 mm. Electrodes for electrochemical studies were embedded in Araldite with an exposed surface area of 1 cm^2. The exposed area of the electrode was abraded by different grades of emery papers (grades 320–1200), then rinsed and dried according to the standard methods.[24] In this study, the solutions used were prepared with reagent grade chemicals. The standard aggressive medium was 3.5 wt% NaCl. The sulfide ions S^{2-} were introduced as Na_2S in this solution to a concentration of 16 ppm.

2.2 Chemical composition of myrrh extract

The plant has been extensively studied and its chemical composition is well known.[25,26] Table 1 demonstrates the main chemical compounds detected as essential oils in myrrh by GCMS.

2.3 Preparation of myrrh

Myrrh extract was obtained directly from myrrh powder. Myrrh was soaked in methanol and left standing for 5 days. The solution was filtered and further distilled at 40 °C to remove the methanol from the myrrh solution extracts and then concentrated to dryness. 1 g was taken from the extract and dissolved in 1000 ml of water to give a concentration of 1000 ppm; the corrosive medium is a solution of 3.5% NaCl + 16 ppm sulfide. Different volumes were taken from the stock solution of myrrh extract (1000 ppm) to prepare different concentrations of extract with corrosive medium.

2.4 Gravimetric method

The corrosion rates of α-brass were calculated by considering the total affected sample area and immersion time. The test samples were weighed and immersed in 50 mL of 3.5% NaCl polluted by 16 ppm sulfide in the absence and presence of varying concentrations of myrrh extract (50–300 ppm), taken in a beaker at temperatures 25–55 °C maintained in a thermostat water bath. The α-brass pieces were weighed and suspended in the beaker with the help of hooks. Each piece was taken out of the test solution, rinsed and dried according to the standard method.[24] The difference in weight for an exposure time of 4 hours was taken as the total weight loss. In order to get good results, the experiments were carried out in triplicate. From the average weight loss results, the corrosion rate, the percentage of inhibition efficiency (% IE) and the degree of surface coverage (θ) were calculated using the following equations:

$$\text{Corrosion rate} = \Delta W/At \quad (1)$$

$$(\%\ \text{IE}) = \theta \times 100 = [(W_1 - W_2)/W_1] \times 100 \quad (2)$$

Table 1 Names, structural formulas and molecular weights for the investigated extract

No.	Name	Chemical structure	Formula	MW	% composition
1	Cyclohexene, 4-ethenyl-4-methyl-3-(1-methylethenyl)-1-(1methylethyl)-, (3*R-trans*)-	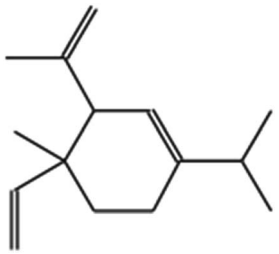	$C_{15}H_{24}$	204	0.3342
2	Longifolene-(V4)	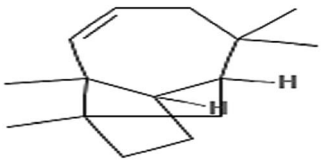	$C_{15}H_{24}$	204	4.048
3	Caryophyllene	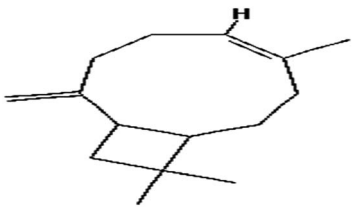	$C_{15}H_{24}$	204	0.2976
4	1,4-Methanoazulene, decahydro-4,8,8-trimethyl-9-methylene-, [1*S*-(1à,3aá,4à,8aá)]-	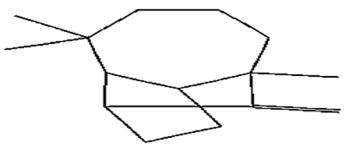	$C_{15}H_{24}$	204	1.047
5	1,6-Cyclodecadiene, 1-methyl-5-methylene-8-(1-methylethyl)-, [s-(*E*,*E*)]-	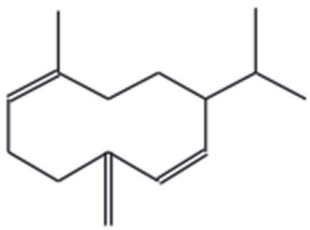	$C_{15}H_{24}$	204	0.3498
6	Naphthalene, 1,2,3,5,6,7,8,8a-octahydro-1,8a-dimethyl-7-(1-methylethenyl)-, [1*S*-(1à,7à,8aà)]-	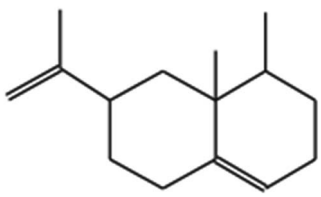	$C_{15}H_{24}$	204	0.3874
7	Benzofuran, 6-ethenyl-4,5,6,7-tetrahydro-3,6-dimethyl-5-isopropenyl-, *trans*-	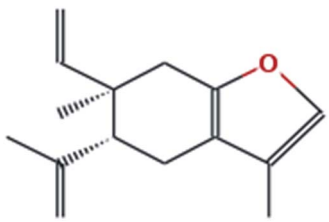	$C_{15}H_{20}O$	216	26.63
8	1*H*-Cycloprop[*e*]azulene, decahydro-1,1,7-trimethyl-4-methylene-, [1a*R*-(1aà, 4aá,7à,7aá,7bà)]		$C_{15}H_{24}$	204	0.5777

Table 1 (*Contd.*)

No.	Name	Chemical structure	Formula	MW	% composition
9	*meso*-Hydrobenzoin	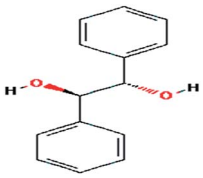	$C_{14}H_{14}O_2$	214	0.3437
10	9(1*H*)-Phenanthrenone, 2,3,4,4a,10,10a-hexahydro-4a-methyl-, *cis*-	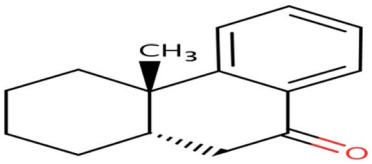	$C_{15}H_{18}O$	214	49.41
11	Benzenemethanol, 3-methoxy-a-phenyl-	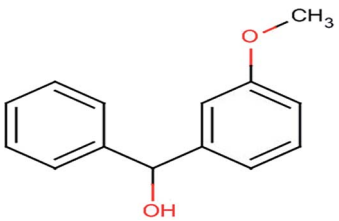	$C_{14}H_{14}O_2$	214	13.79
12	Cyclohexanemethanol, 4-ethenyl-à,à,4-trimethyl-3-(1-methylethenyl)-, [1*R*-(1à,3à,4á)]-	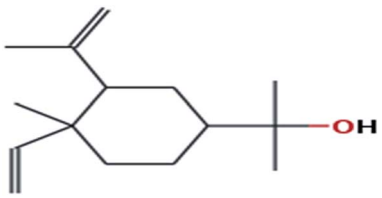	$C_{15}H_{26}O$	222	0.6306
13	Testosterone	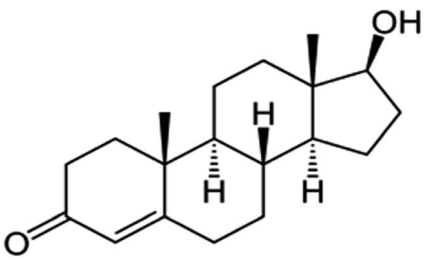	$C_{19}H_{28}O_2$	288	2.154

where ΔW is the weight loss in mg, A is the area of the specimen in cm^2 and t is the exposure time in min, and where W_2 and W_1 are the weight losses for the α-brass sample in the presence and absence of the myrrh extract.

2.5 Electrochemical measurements

We carried out the electrochemical measurements by using a conventional cell with three electrodes. The α-brass was the working electrode, the counter electrode was Pt wire and the reference electrode was a saturated calomel electrode (SCE). The electrochemical measurements were performed using a Gamry Instrument (PCI 300/4) Potentiostat/Galvanostat/ZRA. This instrument includes a Gamry framework system based on the ESA 400. Gamry inclusive DC105 software was used for potentiodynamic polarization measurements, and EFM 140 software was used for electrochemical frequency modulation measurements along with a computer for collecting data and EIS300 software for electrochemical impedance spectroscopy. For plotting, graphing, and fitting data, Echem Analyst 6.03 software was used.

2.6 FTIR analysis

FTIR analysis was carried out to determine the functional groups present in the solutions of the 300 ppm myrrh extract + 3.5% NaCl solution polluted by 16 ppm sulfide, and the other analysis for functional groups present in the 300 ppm myrrh extract + 3.5% NaCl polluted by 16 ppm sulfide after the specimen of α-brass was immersed for 24 h. FTIR analysis was carried out using a FT/IR-4100 type A serial number B117761016.

2.7 UV-visible spectroscopy

The UV-visible absorption spectra of a solution of 3.5% NaCl polluted by 16 ppm sulfide containing 300 ppm myrrh extract before and after immersion of the α-brass for 24 h was studied.

2.8 AFM analysis

The analysis of AFM is one of the major analyses of the surface study, which is used for further investigation of the formation of a protective film on the surface of the α-brass. Atomic force microscopy (AFM) was used to investigate the topography of the α-brass surface immersed for one day in 3.5% NaCl polluted by 16 ppm sulfide in the absence and presence of 300 ppm myrrh extract.

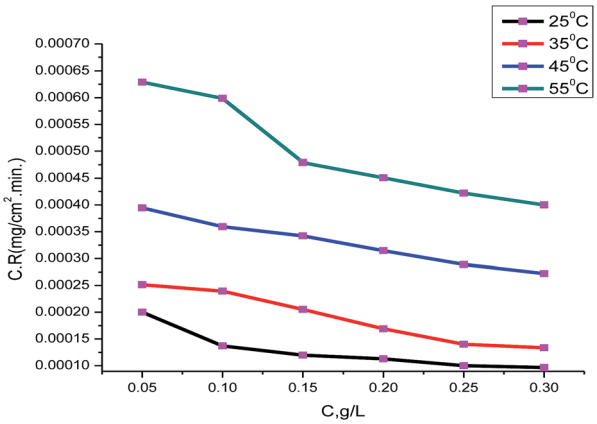

Fig. 1 Corrosion rates of various concentrations of myrrh extract on α-brass in 3.5% NaCl + 16 ppm sulfide at 25–55 °C.

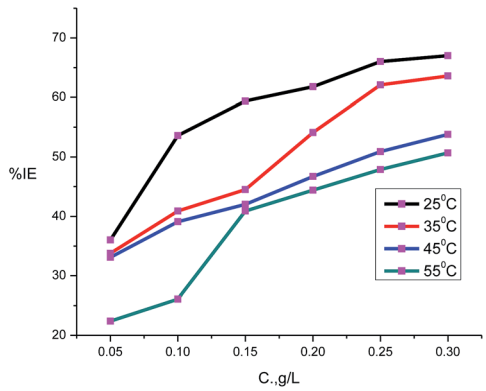

Fig. 2 The variation of inhibition efficiency with myrrh extract concentration of α-brass in 3.5% NaCl + 16 ppm sulfide solutions.

3. Results and discussion

3.1 Gravimetric measurements

The data of the corrosion rate were plotted against different concentrations of the myrrh extract in 3.5% NaCl polluted by 16 ppm sulfide, as shown in Fig. 1. The corrosion rate values of α-brass decrease when the concentration of myrrh extract increases and the magnitude of surface coverage and adsorption by extracts on the α-brass surface increases with concentration of the myrrh extract. Fig. 2 demonstrates that the inhibition efficiency increases with increasing concentration of myrrh extract. Tables 2 and 3 include the experimental data of weight loss (ΔW), percentage of inhibition efficiency (% IE), corrosion rate (C.R.) and degree of surface coverage (θ) for α-brass in 3.5% NaCl + 16 ppm sulfide in the absence and presence of various concentrations of myrrh extract at different temperatures (25–55 °C).

Adsorption isotherm. The action of inhibition in solutions containing 3.5% NaCl +16 ppm sulfide is a result of adsorption at the α-brass/solution interface. The adsorption mode will be dependent on different factors such as the extract composition, chemical changes to the extract and the nature of the surface charge on the metal. For obtaining the adsorption isotherm, the degree of surface coverage (θ) of the extract must be calculated. Many mathematical expressions have thus been developed to take into consideration non-ideal effects. The most used isotherms are Frumkin, Temkin, De Boer, Parsons, Flory–Huggins and Bockris–Swinkels.[27–31] The values of surface coverage (θ) corresponding to different concentrations of myrrh extract at different temperatures (25–55 °C) have been used to determine the best adsorption isotherm. Fig. 3 and 4 confirm that the inhibition process is due to adsorption of the extract components on the ass surface. This is because a straight line is obtained when $\log(C/\theta)$ is plotted against $\log C$ and the linear correlation coefficient of the fitted data is close to 1. Also this was found with the kinetic thermodynamic model of El-Awady. This indicates

Table 2 Data of weight loss of α-brass in a solution of 3.5% NaCl polluted by 16 ppm sulfide for various concentrations of myrrh extract after 180 min, at (25, 35 °C)

	25 °C				35 °C			
Conc., ppm	ΔW, mg cm^{-2}	θ	% IE	C.R., mg cm^{-2} min^{-1}	ΔW, mg cm^{-2}	θ	% IE	C.R., mg cm^{-2} min^{-1}
Blank	0.053	—	—	0.00030	0.066			0.00037
0.05	0.034	0.360	36.0	0.00020	0.044	0.338	33.8	0.00025
0.10	0.025	0.536	53.6	0.00014	0.039	0.409	40.9	0.00024
0.15	0.022	0.594	59.4	0.00012	0.037	0.443	44.3	0.00021
0.20	0.020	0.618	61.8	0.00011	0.030	0.541	54.1	0.00017
0.25	0.018	0.660	66.0	0.00010	0.025	0.621	62.1	0.00014
0.30	0.017	0.672	67.0	0.00009	0.024	0.636	63.6	0.00013

Table 3 Data of weight loss of α-brass in a solution of 3.5% NaCl polluted by 16 ppm sulfide for various concentrations of myrrh extract after 180 min, at (45, 55 °C)

	45 °C				55 °C			
Conc., ppm	ΔW, mg cm^{-2}	θ	% IE	C.R., mg cm^{-2} min^{-1}	ΔW, mg cm^{-2}	θ	% IE	C.R., mg cm^{-2} min^{-1}
Blank	0.106	—	—	0.00059	0.146	—	—	0.00081
0.05	0.071	0.331	33.1	0.00039	0.113	0.224	22.4	0.00063
0.10	0.065	0.391	39.1	0.00036	0.108	0.261	26.1	0.00060
0.15	0.062	0.42	42	0.00034	0.086	0.409	40.9	0.00048
0.20	0.057	0.467	46.7	0.00031	0.081	0.444	44.4	0.00045
0.25	0.052	0.509	50.9	0.00029	0.076	0.479	47.9	0.00042
0.30	0.049	0.538	53.8	0.00027	0.072	0.507	50.7	0.00040

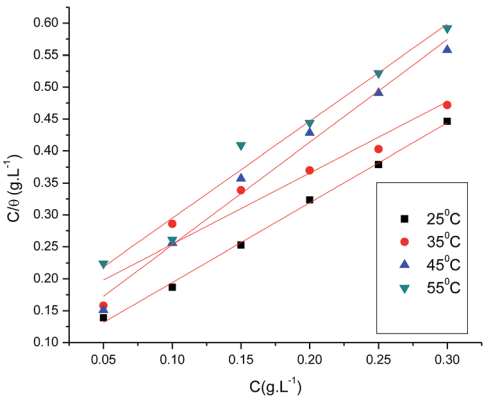

Fig. 3 Langmuir isotherm for myrrh extract adsorption on α-brass in a solution of 3.5% NaCl polluted by 16 ppm sulfide at different temperatures.

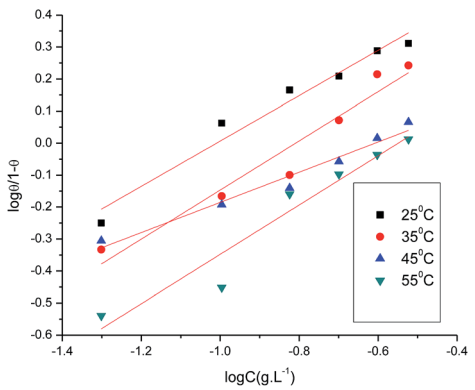

Fig. 4 Kinetic thermodynamic isotherm for myrrh extract adsorption on α-brass in solution of 3.5% NaCl polluted by 16 ppm sulfide at different temperatures.

that the adsorption of the extract molecules obeys the Langmuir adsorption model and the kinetic-thermodynamic model of El-Awady[32,33] which are expressed as:

$$C/\theta = 1/K + C \quad (3)$$

where C is the concentration of myrrh extract and K is the equilibrium constant for the adsorption/desorption process of the extract molecules on the α-brass surface.

$$\log(\theta/1 - \theta) = \log K + y \log C \quad (4)$$

where y is number of myrrh extract molecules occupying one active site, when a value of $1/y$ less than unity implies the formation of a multilayer of the myrrh extract on the α-brass surface, while a value of $1/y$ greater than unity means that a given extract occupies more than one active site.[34–36] θ is the surface coverage. C is the concentration and K is the constant related to the equilibrium constant of the adsorption process. $K_{ads} = K^{1/y}$.

The R^2 values for the Langmuir isotherm were more accurate than those for the kinetic model isotherm. Therefore, the Langmuir adsorption isotherm was found to be the best description of the adsorption behaviour of the myrrh extract on the α-brass surface.

From the obtained data, the values of K_{ads} decrease with increasing temperature. This demonstrates that the strength of adsorption decreases with increasing temperature and the inhibitor species are more readily removed from the α-brass surface.[37–39]

The relationship between the equilibrium constant of adsorption (K) and the standard adsorption free energy (ΔG^0_{ads}) can be calculated from the following eqn (5):[40]

$$K = 1/55.5 \exp[-\Delta G^0_{ads}/RT] \quad (5)$$

The values of free energy of adsorption isotherm which were calculated from the above equation using K values obtained from the Langmuir adsorption and kinetic-thermodynamic model of El-Awady adsorption isotherms are presented in Table 4. The negative values of ΔG^0_{ads} demonstrate spontaneous adsorption of inhibitors on the α-brass surface.[41] In general, values of ΔG^0_{ads} up to −20 kJ mol^{-1} are consistent with physisorption, while those around −40 kJ mol^{-1} or higher are associated with chemisorption as a result of the sharing or transfer of electrons from extract molecules to the metal surface to form a co-ordinate bond.[42]

For the investigated extract, the calculated ΔG_{ads} less than −20 kJ mol^{-1} indicates that the adsorption mechanism of the

Table 4 Parameters of the Langmuir adsorption and kinetic model adsorption for adsorption of myrrh extract on α-brass in 3.5% NaCl for a 180 min immersion period at different temperatures

	Langmuir isotherm					Kinetic model					
Temp. °C	K_{ads}	R^2	$-\Delta G^0_{ads}$ (kJ mol^{-1})	$-\Delta H^0_{ads}$ (kJ mol^{-1})	$-\Delta S^0_{ads}$ (J mol^{-1} K^{-1})	$1/y$	log K_{ads}	R^2	$-\Delta G^0_{ads}$ (kJ mol^{-1})	$-\Delta H^0_{ads}$ (kJ mol^{-1})	$-\Delta S^0_{ads}$ (J mol^{-1} K^{-1})
25	14.44	0.997	16.57	18.53	117.8	1.41	1.010	0.959	15.71	29.93	153.1
35	11.02	0.917	16.43		113.5	1.30	0.810	0.932	15.06		146.1
45	9.88	0.983	16.67		111.0	2.11	0.610	0.960	14.33		139.2
55	6.99	0.968	16.26		106.0	1.29	0.546	0.923	14.38		135.1

myrrh extract on α-brass in 3.5% NaCl solution polluted by 16 ppm sulfide was typical of physisorption.

We calculated the heat of adsorption ΔH^0_{ads} using the Van't Hoff eqn (6):[43]

$$\log K_{ads} = (-\Delta H^0_{ads}/2.303RT) + \text{constant} \quad (6)$$

A straight line obtained by plotting K_{ads} against $1/T$ is shown in Fig. 5; the slope of the straight line gave $(\Delta H^0_{ads}/2.303R)$; from this slope, the values of ΔH^0_{ads} were calculated and are listed in Table 4. Then, the values of ΔS^0_{ads} were calculated using eqn (7):

$$\Delta G^0_{ads} = \Delta H^0_{ads} - T\Delta S^0_{ads} \quad (7)$$

A negative sign of ΔH^0_{ads} demonstrates that the adsorption of the myrrh extract on the α-brass surface is an exothermic process. The results in Table 4 reveal that the value of K_{ads} is not high and when increasing the temperature, it decreased. The results in Table 4 indicate the more positive sign of ΔS_{ads} when the concentration of myrrh extract increases, revealing that the substitution process can be attributed to the increase in the solvent entropy and more positive water desorption entropy. It also inferred that there is an increase in disorder due to there being more water molecules which can be desorbed from the α-brass surface by one molecule from myrrh extract.[44,45] This is deduced from the principles of thermodynamics, since the adsorption is an exothermic process and accompanied by a decrease of entropy.[46]

The effect of temperature on the efficiency of inhibition. From our investigation, the protection efficiency decreases with an increase in temperature. This could be due to the weakness of the adsorption process at higher temperature, suggesting physical adsorption of the myrrh extract on the α-brass surface. Also, the data of Tables 2 and 3 revealed that the weight loss of α-brass increases with increasing the temperature, indicating that the rate of corrosion of the alloy increases with increasing the temperature. The dependence of the rate of corrosion (C.R.) on the temperature can be expressed by the Arrhenius eqn (8):

$$\text{C.R.} = A\exp\left(-E^*_a/RT\right) \quad (8)$$

where $(-E^*_a)$ is the apparent activation energies for the corrosion process in the absence and presence of the myrrh extract and A = pre-exponential factor.

Fig. 6 demonstrates Arrhenius plots of the corrosion of α-brass in 3.5% NaCl polluted by 16 ppm sulfide with and without different concentrations of the myrrh extract. The linear regression (R^2) is close to 1 which led to the conclusion that the corrosion of α-brass in 3.5% NaCl solution polluted by 16 ppm sulfide ions can be studied using the kinetic model. From Table 5 the data of E^*_a indicates that E^*_a values increase in the

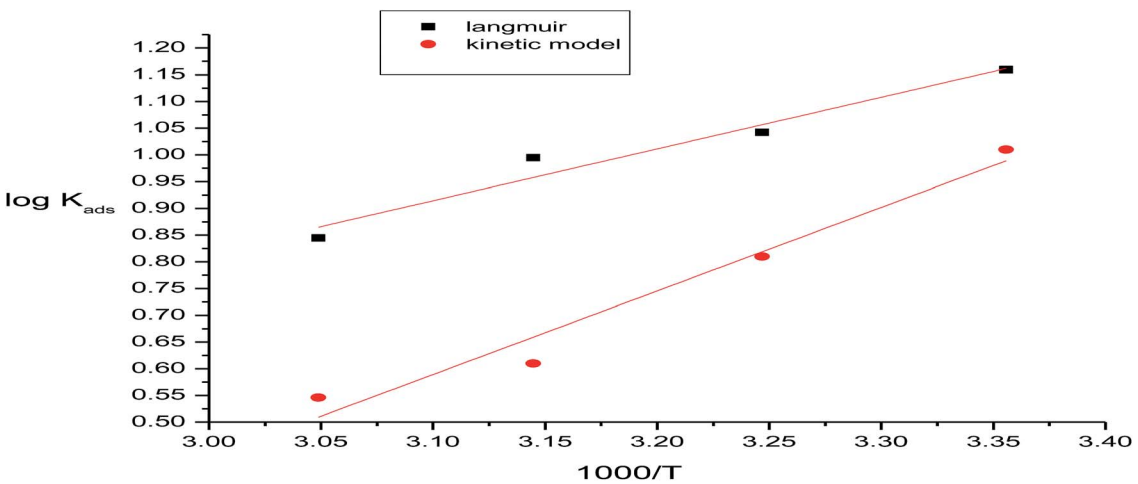

Fig. 5 log K_{ads} *vs.* $(1/T)$ curves for the corrosion of α-brass in 3.5% NaCl polluted by 16 ppm sulfide in the absence and presence of different concentrations of myrrh extract at different temperatures.

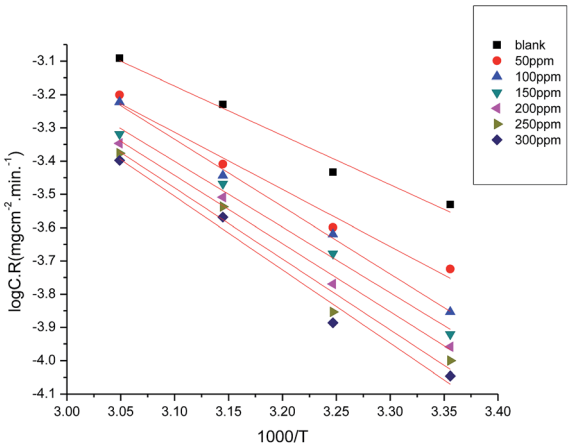

Fig. 6 Arrhenius plots (log C.R. *vs.* 1/*T*) for α-brass in 3.5% NaCl + 16 ppm sulfide without and with different concentrations of myrrh extract.

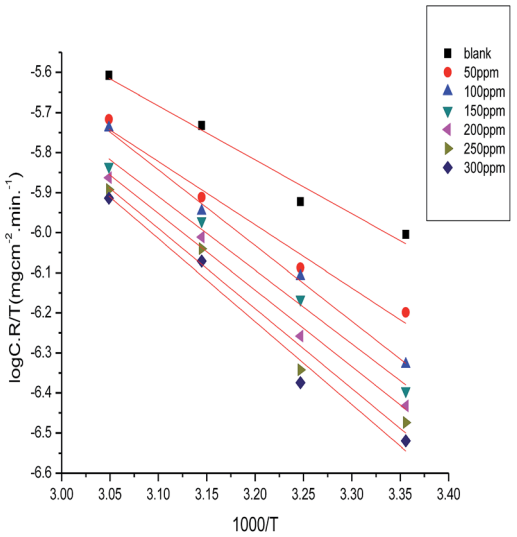

Fig. 7 Plots of log C.R./*T* *vs.* 1000/*T* for α-brass in 3.5% NaCl polluted by 16 ppm sulfide without and with different concentrations of myrrh extract at 25 °C.

presence of the myrrh extract compared to in its absence. From these data we can say: the molecules of myrrh extract are adsorbed on the α-brass surface physically.

In the process of corrosion, the entropy and enthalpy of activation were calculated from the transition state theory as demonstrated in eqn (9):

$$\text{C.R.} = (RT/Nh)\exp(\Delta S^*/R)\exp(-\Delta H^*/RT) \quad (9)$$

where N is Avogadro's number and h is Planck's constant.

ΔS^* is the entropy of activation and ΔH^* is the enthalpy of activation. Fig. 7 shows a plot of log(C.R./T) *vs.* (1/T). We obtained straight lines with slopes of ($\Delta H^*/2.303R$) and intercepts of (log R/Nh + $\Delta S^*/2.303R$). ΔH^* and ΔS^* values were calculated and are listed in Table 5. The negative values of ΔH^* demonstrate that the corrosion process is an exothermic one. When the values of enthalpy of activation are lower than 41.86 kJ mol^{-1}, this demonstrates physical adsorption, and when the values are approaching 100 kJ mol^{-1}, this reveals chemical adsorption.[47] In our study, the values of ΔH^* are lower than 41.86 kJ mol^{-1}, confirming physical adsorption. The values of the entropy (ΔS^*) in the presence of the myrrh extract are negative; this reflects that the activated complex in the rate determining step represents an association rather than a step of dissociation. This demonstrates that the initial state was of lower order than the activated molecules.[48]

Table 5 Kinetics parameters of the Arrhenius equation and the transition state equation

Conc. ppm	E_a^*, kJ mol^{-1}	$-\Delta H^*$, kJ mol^{-1}	$-\Delta S^*$, J mol^{-1} K^{-1}
Blank	28.39	25.78	226.49
50	32.84	30.24	215.02
100	38.76	36.16	197.86
150	37.70	35.21	201.43
200	39.10	36.64	197.97
250	40.86	38.27	193.65
300	42.26	39.67	189.78

3.2 Open circuit potential measurements

The variation of the open circuit potential (OCP) of α-brass electrodes as a function of time was studied against a saturated calomel electrode (SCE) in the absence and presence of various concentrations of myrrh extract as indicated in Fig. 8. This study demonstrated that the corrosion potential (E_{corr}) of the α-brass electrode in 3.5% NaCl solution polluted by 16 ppm sulfide ions tends to shift to a more noble direction until a steady state potential is established. This suggests that the kinetics of the anodic reaction of α-brass in 3.5% NaCl solution polluted by 16 ppm sulfide ions was affected more strongly in the presence of the myrrh extract.[49,50]

3.3 Potentiodynamic polarization

Potentiodynamic polarization curves for α-brass in 3.5% NaCl solution polluted by 16 ppm sulfide ions in the absence and

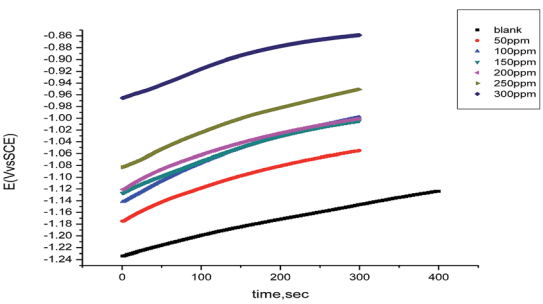

Fig. 8 Potential–time curves for α-brass in 3.5% NaCl solution with 16 ppm sulfide ions in the absence and presence of different concentrations of myrrh extract at 25 °C.

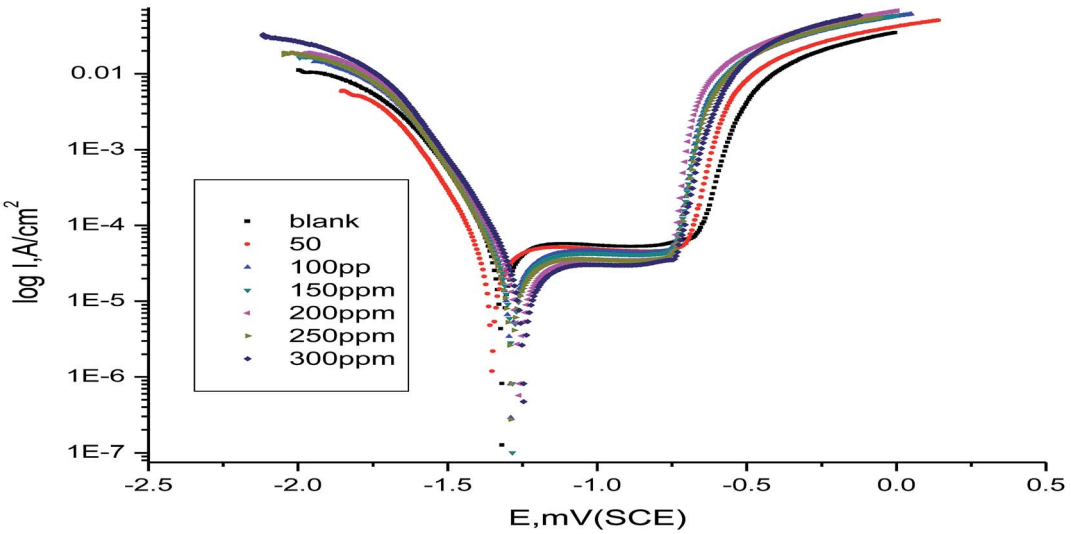

Fig. 9 Anodic and cathodic polarization curves for α-brass in 3.5% NaCl solution polluted by 16 ppm sulfide ions in the absence and presence of different concentrations of myrrh extract at 25 °C.

presence of different concentrations of myrrh extract at 25 °C are shown in Fig. 9, and the polarization parameters [E_{corr}, i_{corr}; anodic and cathodic Tafel slopes (β_a, β_c) and resistance polarization (R_P)] are registered in Table 6. Both the anodic and cathodic Tafel slopes were slightly changed on increasing the concentration of myrrh extract. This means that the mechanism of inhibition not in the presence and absence of myrrh extract affects both the cathodic and anodic reactions, *i.e.* it is a mixed-type inhibitor. The E_{corr} values show that the myrrh extract behaves as a mixed type, because the variation is small in the E_{corr}.[51–53] The results from Fig. 9 and Table 6 demonstrate that the presence of myrrh extract and the increase of its concentration decrease the values of the corrosion rate and raise the values of R_P and IE%. We calculated the degree of surface coverage (θ) and inhibition efficiency (% IE) using the following equation:

$$\% \text{ IE} = \theta \times 100 = [1 - (i_{corr}/i^0_{corr})] \times 100 \quad (10)$$

where, i^0_{corr} and i_{corr} are the corrosion current densities without and with the myrrh extract, respectively. The anodic polarization curves show three important regions; namely, the Tafel region at lower overpotentials extending to the peak current density due to the dissolution of copper to Cu^+ ions, a region of decreasing current density until a minimum (i_{min}) is reached due to the formation of CuCl, and a region of sudden increase in current density leading to a limiting value (i_{lim}), due to the formation of $CuCl_2$.[54,55] Tafel polarization plots were obtained using a scan rate of 1 mV s^{-1} in the potential range from −1000 to +1000 mV with respect to the open circuit potential (E_{ocp}).

3.4 Electrochemical impedance spectroscopy

The impedance data of the α-brass electrode in the presence of different concentrations of myrrh extract were studied using the equivalent circuit shown in Fig. 10. This circuit includes constant phase elements (CPE) in place of capacitors to represent various types of non-homogeneities typical of corroding electrodes such as roughness of the surface, insufficient polishing, grain boundaries and impurities of the surface.[56] The impedance of α-brass is dependent on frequency, and can be expressed mathematically using two parameters, Y_0 and n as:[57]

$$Z_{CPE} = Y_0^{-1}(j\omega)^{n-1} \quad (11)$$

where Y_0 is the CPE coefficient, $j^2 = -1$ is the imaginary number and ω is the sine wave modulation angular frequency and

Table 6 Potentiodynamic polarization parameters for α-brass corrosion in 3.5% NaCl polluted by 16 ppm sulfur ions in the absence and presence of different concentrations of myrrh extract at 25 °C

Conc., ppm	$-E_{corr}$, mV *vs.* SCE	i_{corr}, μA cm^{-2}	R_P, ohm	β_a, mV dec^{-1}	$-\beta_c$, mV dec^{-1}	θ	% IE	mpy
Blank	1320	92.7	29.03	197.0	252			33.09
50	1290	54.8	32.79	190.0	220.0	0.409	40.9	25.08
100	1290	52.5	33.20	139.8	187.3	0.433	43.3	20.60
150	1280	49.3	34.10	164.0	187.0	0.468	46.8	19.23
200	1260	37.0	36.79	196.0	189.6	0.601	60.1	15.87
250	1290	33.4	42.46	174.4	176.0	0.640	64.0	15.36
300	1250	30.5	65.38	190.0	166.3	0.670	67.0	13.53

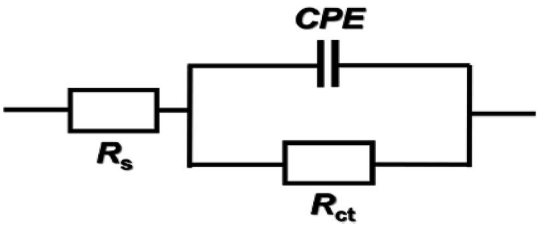

Fig. 10 Equivalent circuit proposed to fit the EIS experimental data.

equals $2\pi f$, where f is the AC frequency. In real experimental conditions, the n values are between 0 and 1 as a result of the influence of many factors such as electrode roughness, surface heterogeneity, and the dielectric constant.[58] The slightly lower values of n for the blank compared to the inhibited systems suggest that the α-brass surface is relatively more homogeneous, which may be due to uniform adsorption of the myrrh extract molecules on the α-brass surface. We calculated the double layer capacitance (C_{dl}) from the following equation.[59]

$$C_{dl} = Y_0\omega^{n-1}/\sin[n(\pi/2)] \quad (12)$$

From the following equation we calculated the degree of surface coverage (θ) and the inhibition efficiency (% IE)

$$\%\ \mathrm{IE} = \theta \times 100 = [1 - (R_{ct}^0/R_{ct})] \times 100 \quad (13)$$

where R_{ct} and R_{ct}^0 are the charge transfer resistances with and without myrrh extract, respectively; θ and % IE are also listed in Table 7. The interface of the α-brass surface and the aqueous electrolyte is a complex process consisting of a line of positively and negatively charged ions. Also, it contains a coating or film formation on the surfaces. Capacitance is the result of an electrical double layer (C_{dl}), charge transfer resistance (R_{ct}), solution resistance (R_s), and diffusion of ions; movement of charge in or away from the α-brass surface and adsorption of cations and anions gives various impedances. The data which are listed in Table 7 show impedance for α-brass in 3.5% NaCl polluted by 16 ppm of sulfide ions without and with various concentrations of myrrh extract. The diagrams of impedance (Nyquist and Bode plots) obtained for α-brass in the presence of various concentrations of myrrh extract are depicted in Fig. 11. The charge transfer resistance of the corrosion reaction increases as a result of increasing the diameter of the semicircle which increases with increasing the concentration of myrrh

Table 7 EIS parameters for corrosion of α-brass in 3.5% NaCl polluted by 16 ppm sulfide ions in the absence and presence of different concentrations of myrrh extract at 25 °C

Conc., ppm	R_{ct}, Ω cm^{-2}	R_S, Ω cm^{-2}	$Y_0 \times 10^6$, μΩ^{-1} S^n	n	$C_{dl} \times 10^5$, F cm^{-2}	θ	% IE
Blank	5.95×10^3	9.38×10^{-3}	170	0.716	1.24	—	—
50	9.15×10^3	12.68×10^{-3}	130.2	0.742	0.716	0.349	34.9
100	10.32×10^3	10.97×10^{-3}	101.8	0.791	0.110	0.423	42.3
150	11.2×10^3	12.37×10^{-3}	107.6	0.796	0.119	0.469	46.9
200	15.1×10^3	17.93×10^{-3}	98.82	0.793	0.111	0.606	60.6
250	16.41×10^3	12.41×10^{-3}	117.4	0.788	0.140	0.637	63.7
300	17.9×10^3	18.89×10^{-3}	172.9	0.731	0.257	0.667	66.7

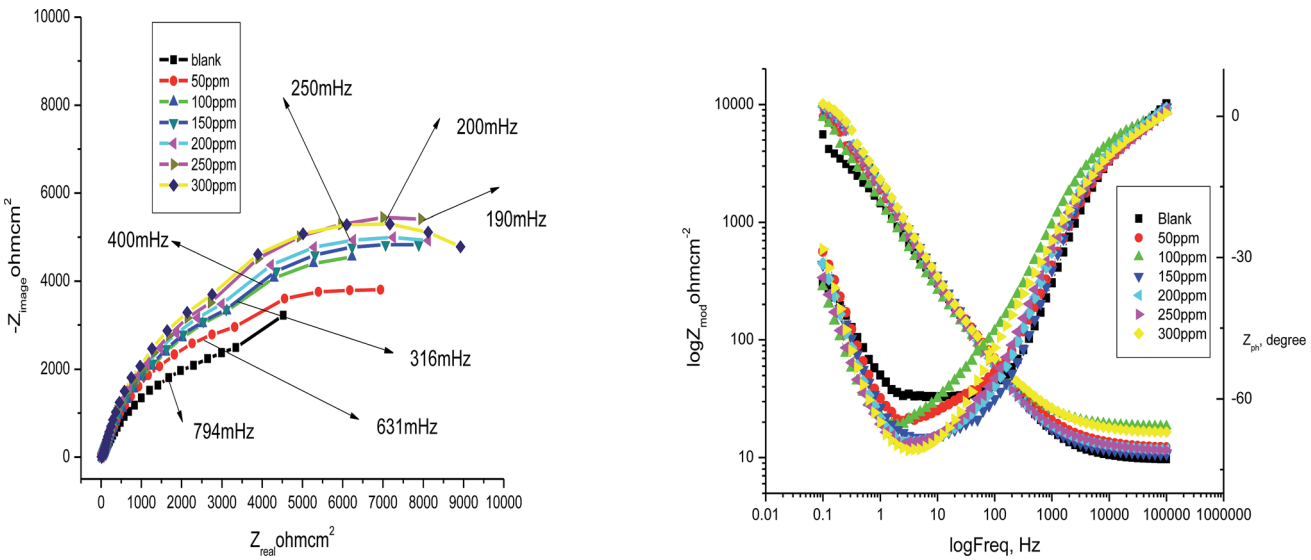

Fig. 11 Nyquist and Bode plots for corrosion of α brass in 3.5% NaCl polluted in the absence and presence of different concentrations of myrrh extract at 25 °C.

extract. This is attributed to high resistance shown by the adsorbed myrrh extract components at the α-brass alloy–solution interface.[60] The Nyquist plots do not close as a semicircle, as expected from the theory of EIS. The deviation from an ideal semicircle was generally attributed to the frequency dispersion as well as to the inhomogeneities of the surface.[61,62] The decrease in C_{dl} in comparing with that in the blank solution (without different concentrations of myrrh extract) is a result of the decreasing local dielectric constant and/or an increase in the thickness of the electrical double layer. This is because of the adsorption of extract molecules at the alloy/solution interface.[63] The obtained impedance diagrams have an almost semicircular appearance, indicating a charge transfer process which mainly controls the corrosion of α-brass.[64,65] Electrochemical impedance spectroscopy was studied at corrosion potentials, E_{corr}, over a frequency range of 10^5 Hz to 0.1 Hz with a signal amplitude perturbation of 10 mV.

3.5 Electrochemical frequency modulation (EFM) measurements

The electrochemical frequency modulation technique is considered to be a non-destructive technique and a rapid test, which directly gives data of the corrosion current without knowledge of the constants of Tafel, and this technique has great strength because of the causality factors, which are considered as an internal check on the validity of the EFM measurements.[66] This technique has a small AC signal like EIS, but there is a difference between the two techniques, because EFM has two sine waves (at different frequencies) which are applied to the cell simultaneously. The system responds in a nonlinear way to the potential excitation, because the current is a nonlinear function of potential. The current response contains the input frequencies, and also contains frequency components which are the sum, difference, and multiples of the two input frequencies. The two frequencies must be small, integer multiples of a base frequency that determines the length of the experiment. Table 8 indicates the corrosion parameters such as inhibition efficiency, Tafel constants (β_a, β_c), corrosion current density (μA cm^{-2}), and causality factors (CF-2, CF-3) at different concentrations of myrrh extract in 3.5% NaCl polluted by 16 ppm sulfide ions at 25 °C. The causality factors in Table 8 demonstrate that the measured values are of good quality. The standard data for CF-2 and CF-3 are 2.0 and 3.0, respectively. If the causality factor data differ significantly from the theoretical values of 2.0 and 3.0, then it can be demonstrated that the measured values are influenced by noise. If the experimental causality factors are approximately equal to the theoretical values, there is a causal relationship between the perturbation signal and the response signal. Then, the values are assumed to be reliable.[67] Table 8 indicates that, by increasing the concentrations of myrrh extract, the corrosion current densities decrease. Also, the inhibition efficiencies increase by increasing the myrrh extract concentrations. The inhibition efficiencies (% IE_{EFM}) depicted in Table 8 were calculated using eqn (14):

$$\%\ IE_{EFM} = \theta \times 100 = [1 - (i_{corr}/i^0_{corr})] \times 100 \quad (14)$$

where i^0_{corr} and i_{corr} are the corrosion current densities in the absence and presence of myrrh extract. The difference in the inhibition efficiencies (% IE_{EFM}) obtained with the different techniques are a result of the variations between the individual techniques and the different models that were used for the interpretation.[68,69] We performed the EFM technique with applying a potential perturbation signal of amplitude 10 mV with two sine waves of 2 and 5 Hz. The choice for the frequencies of 2 and 5 Hz was based on three arguments (Fig. 12).[70]

3.6 AFM (atomic force microscopy)

Scanning force microscopy (SFM) or atomic force microscopy (AFM) is a very high-resolution type of scanning probe microscopy, with demonstrated resolution on the order of fractions of a nanometer, more than 1000 times better than the optical diffraction limit.[71,72] Fig. 13 depicts the morphologies of the α-brass specimens after immersion for one day in 3.5% NaCl solution polluted by 16 ppm sulfide without and with 300 ppm of myrrh extract. Table 9 demonstrates the S_a (average roughness), S_q (root-mean-square roughness), and *P–V* value (the maximum peak-to-valley height values). The average roughness S_a of α-brass in 3.5% NaCl solution polluted by 16 ppm sulfide without myrrh extract was calculated as 694.87 nm by atomic force microscopy (Fig. 13A). In the presence of the myrrh extract, a smoother surface was obtained and the S_a value decreased to 208.34 nm (Fig. 13B) as a consequence of low corrosion damage and the protective formation of a myrrh extract layer on the steel surface. It can be clearly observed that in the absence of the myrrh extract, the α-brass surface was seriously corroded with areas of uniform corrosion. In the presence of the myrrh extract, however, the specimen surface was more smooth. This is due to the involvement of myrrh extract molecules in the interaction with the reaction sites of the

Table 8 Electrochemical kinetic parameters obtained using the EFM technique for α-brass in 3.5% NaCl solutions with myrrh extract at 25 °C

Conc., ppm	i_{corr}, μA cm^{-2}	β_a, mV dec^{-1}	$-\beta_c$, mV dec^{-1}	CF-2	CF-3	θ	% IE	mpy
Blank	5.62	120.2	138.3	1.90	2.80	—	—	2.753
50	3.35	135.3	162.2	1.87	2.77	0.404	40.4	2.46
100	3.20	140.2	170.0	2.06	3.20	0.431	43.1	2.331
150	2.97	160.0	177.0	1.69	2.98	0.471	47.1	1.75
200	2.23	170	142.0	1.81	2.77	0.603	60.3	1.56
250	1.98	168	174.0	1.88	3.90	0.648	64.8	1.18
300	1.83	178	164.0	2.30	3.40	0.674	67.4	1.09

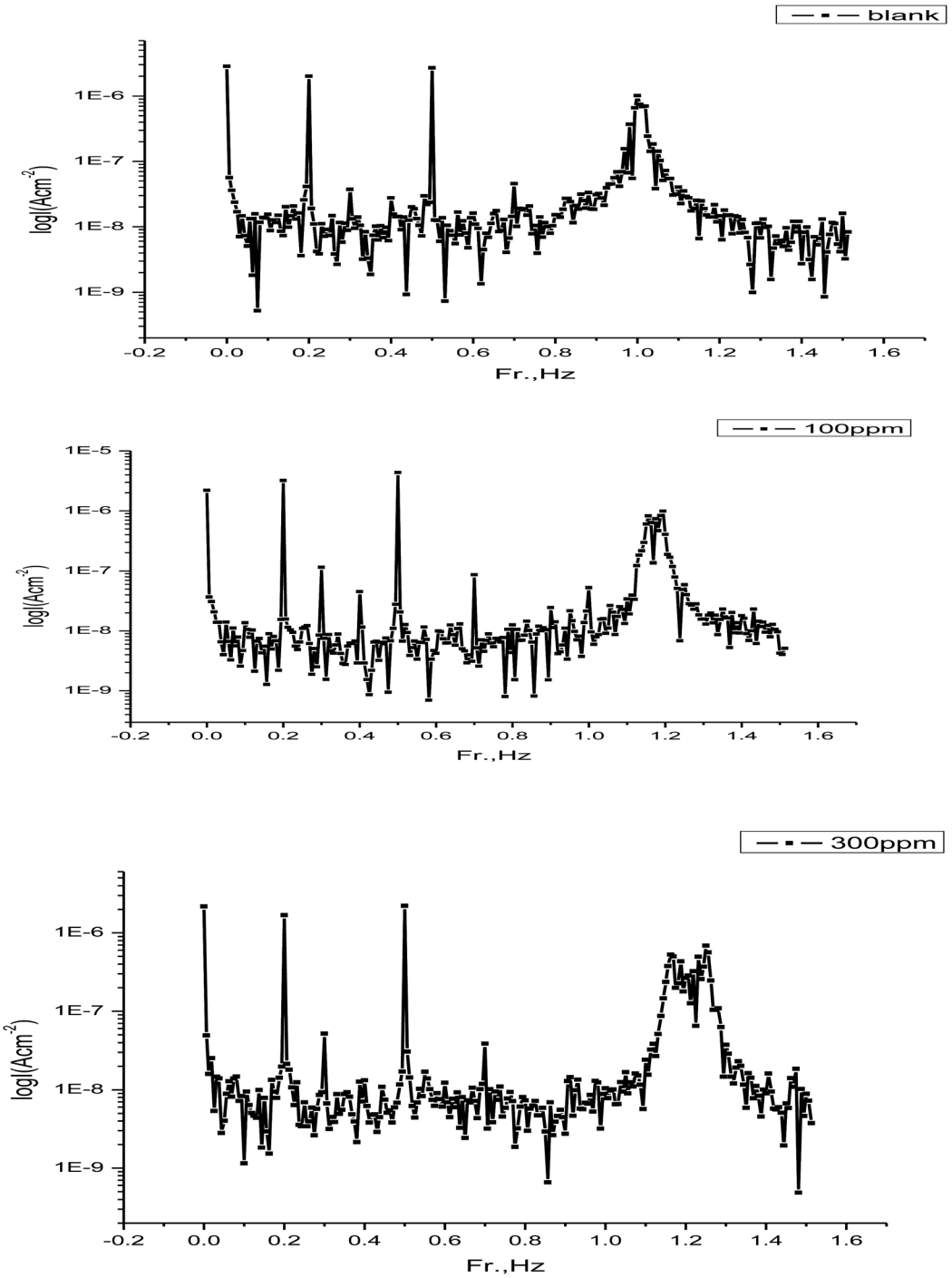

Fig. 12 EFM intermodulation spectra (current *vs.* frequency) without and with different concentrations of myrrh extract for corrosion of α-brass in 3.5% NaCl solution polluted at 25 °C.

α-brass, resulting in a decrease in the contact between the alloy and the aggressive medium and the sequentially exhibited excellent inhibition effect.

3.7 Fourier transform infrared spectroscopy analysis (FT-IR)

To identify the functional groups present in the myrrh extract we used Fourier transform infrared spectroscopy analysis (FT-IR) using liquid samples. Fig. 14 and 15 demonstrate the FT-IR spectra of the myrrh extract and the corrosion products which are present. The results obtained from our study demonstrated that corrosion inhibition takes place through an adsorption process. The spectrum of the 300 ppm of myrrh extract in 3.5% NaCl solution polluted by 16 ppm sulfide ions (Fig. 14) shows that broad peaks appeared at 3424.96, 1644.98, 1386.57 and 2102.03 cm^{-1} which correspond to the O–H, C=O, C=C and aliphatic C–H stretching vibration frequencies, respectively.

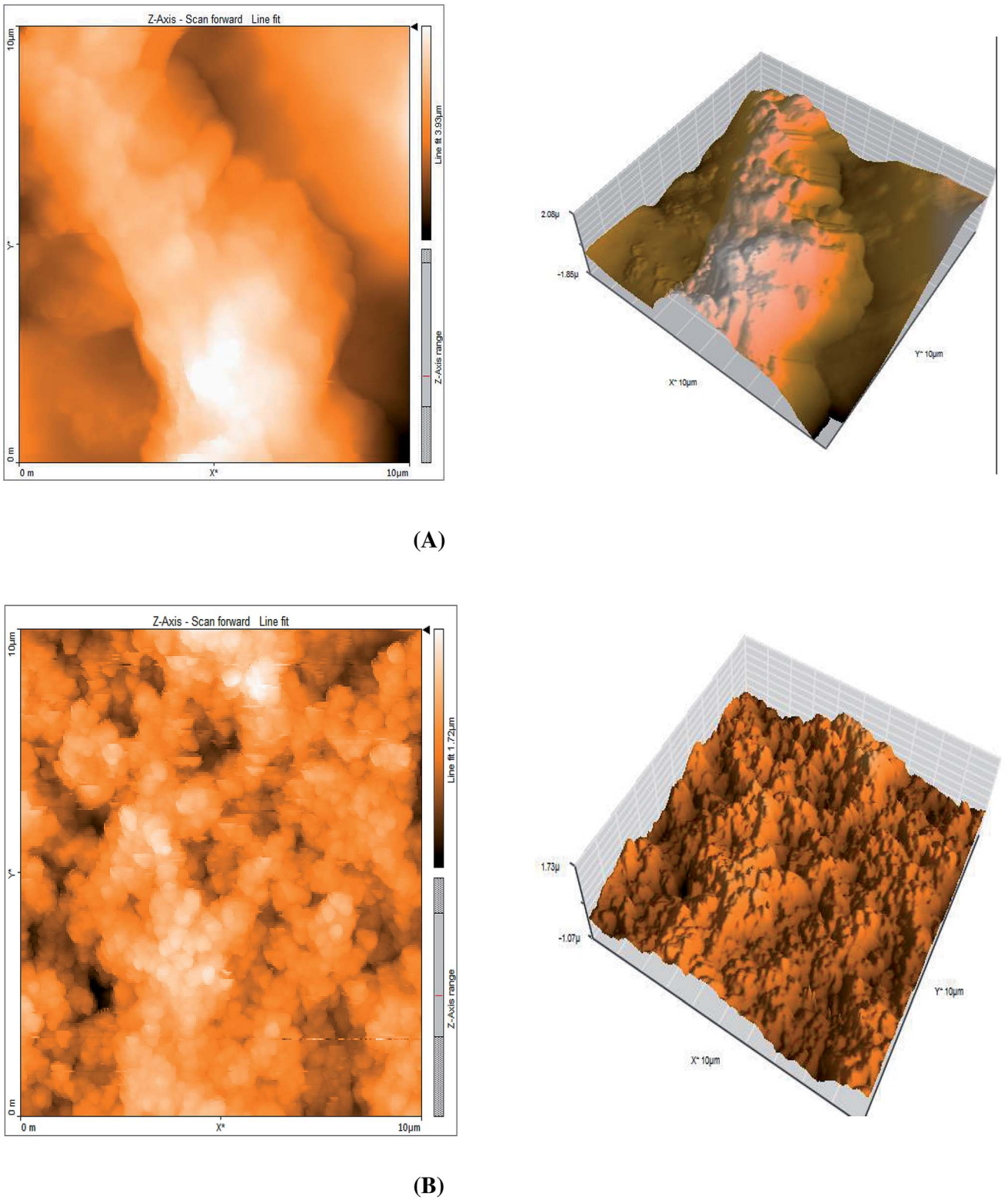

Fig. 13 (A) Surface of the α-brass electrode imaged using atomic force microscopy after 24 h immersion in 3.5% NaCl solution polluted by 16 ppm sulfur ions. (B) Surface of the α-brass electrode imaged using atomic force microscopy after 24 h immersion in 3.5% NaCl solution polluted by 16 ppm sulfur ions with 300 ppm myrrh extract.

From the results, there is a shift in the spectra of the myrrh extract when α-brass was immersed in it to form a corrosion product (Fig. 15). This indicates that there is an interaction between the extract and the α-brass substrate which resulted in an inhibition process. The shifts in the spectra are considered to be a result of the interaction between the myrrh extracts and the

Table 9 The morphology data of the surface of the α-brass after immersion for 24 h in 3.5% NaCl solution polluted by 16 ppm sulfide ions without and with 300 ppm of myrrh extract was examined in the light of an atomic force microscope

Samples	S_q (nm)	S_a (nm)	Maximum peak-to-valley height (nm)
1-α-brass immersed in 3.5% NaCl solution polluted (blank)	810.95	694.87	4106
3-α-brass immersed in 3.5% NaCl solution polluted + 300 ppm (myrrh extract)	259.32	208.34	1769

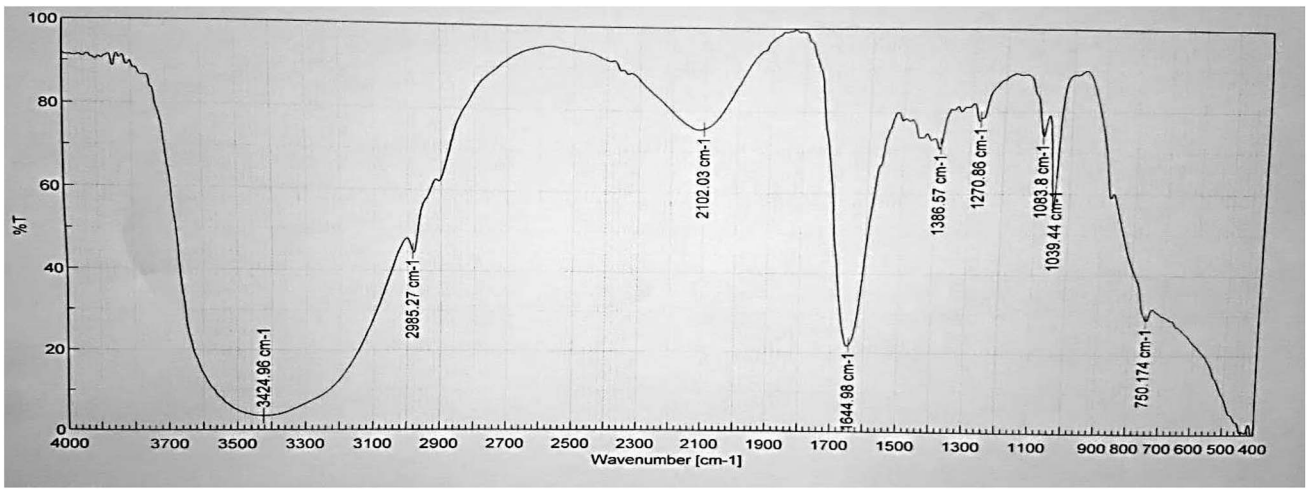

Fig. 14 FT-IR spectrum of the myrrh extract before adsorption on the α-brass surface.

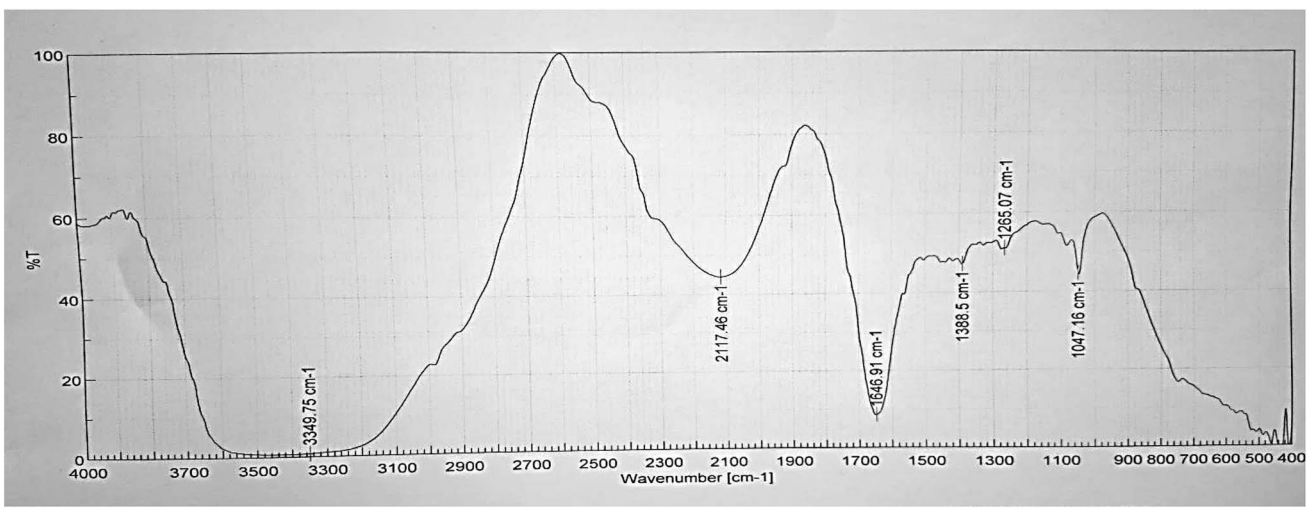

Fig. 15 FT-IR spectrum of the myrrh extract after adsorption on the α-brass surface.

α-brass, occurring through the functional groups present in them. So, it can be affirmed that the functional group has coordinated with the alloy formed on the surface resulting in the formation of a Cu^{2+} extract complex on the alloy surface, which promotes the inhibition of the alloy sample.

3.8 UV-visible analysis

Visible absorption spectra obtained from 3.5% NaCl solution polluted by 16 ppm sulfide ions containing 300 ppm myrrh extract before and after the α-brass immersion are shown in Fig. 16, and confirmed the possibility of the formation of an inhibitor–Cu complex. The electronic absorption spectra of the myrrh extract before immersion have an absorption maximum at 240 nm which can be attributed to π–π* and "n–π*" transitions. After 24 h immersion of the α-brass, the change in the position of the absorption maximum or the change in the absorbance values indicate the complex formation between the two species in solution. Furthermore, there is no change in the

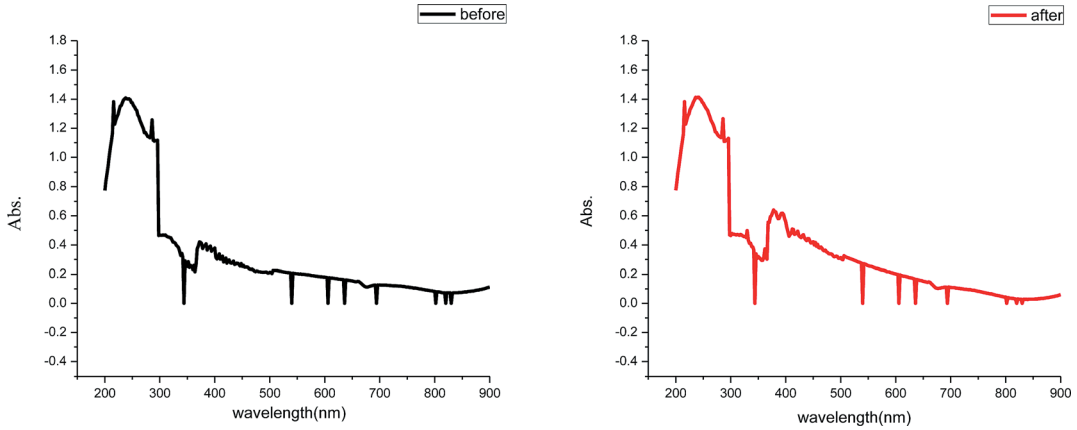

Fig. 16 UV-Visible spectra of the solution of 3.5% NaCl polluted by 16 ppm sulfide ions containing 300 ppm myrrh extract before and after 24 h of α-brass immersion.

shape of the absorption spectra. These experimental findings prove the formation of a complex between Cu^{2+} and the myrrh extract and confirm the inhibition of the α-brass corrosion.[73]

4. Conclusions

The inhibition effects of the myrrh extract on the corrosion of α-brass in 3.5% NaCl solution polluted by 16 ppm sulfide were studied in the present work using weight loss measurements, electrochemical techniques (potentiodynamic polarization measurements, EIS and EFM) and AFM surface analysis, resulting in the following experimental evidences:

(1) From the weight loss measurements, the corrosion rate decreased by addition of myrrh extract to α-brass in 3.5% NaCl solution polluted by 16 ppm sulfide, while the inhibition efficiency increased when increasing the myrrh extract concentration and decreased with temperature.

(2) The adsorption isotherm of the myrrh extract on the α-brass surface can be described by the Langmuir and kinetic thermodynamic adsorption isotherms. The obtained values of ΔG^0_{ads} from the Langmuir and kinetic thermodynamic adsorption isotherms indicate that the physisorption mechanism was an adsorption process.

(3) From the potentiodynamic study, the myrrh extract is found to be a mixed type inhibitor.

(4) AFM indicated that the morphology of the α-brass surface in the presence of the myrrh extract is less damaged due to the formation of the smooth protective film.

(5) Based on the results of weight loss, potentiodynamic polarization measurements, EIS and EFM, the myrrh extract was shown to be an effective inhibitor in 3.5% NaCl polluted by 16 ppm sulfide on α-brass.

References

1 E. M. Sherif, R. M. Erasmus and J. D. Comins, *J. Colloid Interface Sci.*, 2007, **309**(2), 470–477.
2 M. G. Fontana, *Corrosion Engineering*, Mc Graw-Hill International, New York, 1987.
3 A. S. El-Amoush, *J. Alloys Compd.*, 2008, **448**, 257–262.
4 A. Pola, M. Gelfi, L. E. Depero and R. Roberti, *Eng. Failure Anal.*, 2008, **15**, 54.
5 R. Ravichandran and N. Rajendran, *Ap. Surf. Sci.ce*, 2005, **241**, 449–458.
6 G. Kear, B. D. Barker, K. R. Stokes and F. C. Walsh, *J. Appl. Electrochem.*, 2004, **34**, 659–669.
7 W. A. Badawy, M. M. El-Rabiee, N. H. Helal and H. Nady, *Electrochim. Acta*, 2012, **71**, 50–57.
8 G. Kear, B. D. Barker, K. R. Stokes, F. C. Walsh, I. Part and I. I. Part, *J. Appl. Electrochem.*, 2004, **34**, 1235–1240.
9 D. Féron, *"Corrosion behaviour and protection of copper and aluminium alloys in seawater"*, Woodhead Publication, Cambridge, England, 1st edn, 2007.
10 P. N. L. Lens and L. Hulshoff Pol, *Environmental technologies to treat sulfur pollution*, IWA Publication, 1st edn, England, 2000.
11 H. Nady, M. M. El-Rabiei and M. Samy, *Egypt. J. Pet.*, 2017, **26**, 79–94.
12 K. Rahmouni, M. Keddam, A. Srhiri and H. Takenouti, *Corr. Sci.ce*, 2005, **47**, 3249–3266.
13 M. A. Elmorsi and A. M. Hassanein, *Corros. Sci.*, 1999, **41**, 2337–2352.
14 M. El Bakri, R. Touir, A. Tazouti, N. Dkhireche, M. Ebn Touhami, A. Rochdi and A. Zarrouk, *Arabian J. Sci. Eng.*, 2016, **41**, 75–88.
15 L. Yohai, W. H. Schreiner, M. Vázquez and M. B. Valcarce, *J. Solid State Electrochem.*, 2015, **19**, 1559–1568.
16 L. Babouri, K. Belmokre, A. Abdelouas, J. F. Bardeau and Y. El Mendili, *Int. J. Electrochem. S.ci*, 2015, **10**, 7818–7839.
17 A. C. Jayasree and R. Ravichandran, *Int. J. Curr. Microbiol. Appl. Sci.*, 2014, **3**, 515–526.
18 J. R. Xavier and R. Nallaiyan, *J. Solid State Electrochem.*, 2012, **16**, 391–402.
19 I. Batlle and J. Tous, *Carob Tree. Ceratonia siliqua L, Promoting the Conservation and Use of Underutilized and Neglected Crops*, Plant Genetic Resources Institute, Rome, 1997, p. 92.

20 F. S. De Souza, C. Giacomelli, R. S. Gonçalves and A. Spinelli, *Mater. Sci. Eng., C*, 2012, **32**(8), 2436–2444.
21 A. S. Fouda, K. Shalabi and A. A. Idress, *Green Chem. Lett. Rev.*, 2015, **8**, 17–29.
22 Z. V. P. Murthy and K. Vijayaragavan, *Green Chem. Lett. Rev.*, 2014, **7**, 209–219.
23 O. E. Nnabuk, A. O. Stevens and N. A. Ibiam, *Green Chem. Lett. Rev.*, 2010, **3**, 165–172.
24 ASTM, G 31–72, *American Society for Testing and Materials*, Philadelphia, PA, 1990.
25 S. A. Gadir and I. M. Ahmed, *J. Chem. Pharm. Res.*, 2014, **6**(7), 151–156.
26 L. O. Hanuš, T. Řezanka, V. M. Dembitsky and A. Moussaieff, *Biomed. Pap.*, 2005, **149**(1), 3–28.
27 N. Harckerman and R. M. Hurd, *1st International Congress on Metallic Corrosion*, Butterworths, London, vol. 166, 1962.
28 Z. M. Hadi and J. Al-Sawaad, *J. Mater. Environ. Sci.*, 2011, **2**(2), 128–147.
29 B. Zerga, M. Sfaira, M. Taleb, M. Ebn Touhami, B. Hammouti, A. Attayibat, S. Radi and A. T. Benjelloun, *Der Pharma Chemica*, 2012, **4**(5), 1887–1896.
30 A. Amin, K. F. Khaled, Q. Mohsen and A. Arida, *Corros. Sci.*, 2010, **52**, 1684–1695.
31 S. A. Umoren, O. Ogbobe, I. O. Igwe and E. E. Ebenso, *Corros. Sci.*, 2008, **50**, 1998–2006.
32 M. P. Chakravarthy and K. N. Mohana, *ISRN Corros.*, 2014, **2014**, 1–13.
33 A. A. El-Awady, B. A. Abd-El-Nabey and S. G. Aziz, *J. Electrochem. Soc.*, 1992, **139**, 2149–2154.
34 A. K. Singh, S. K. Shukla, M. Singh and M. A. Quraishi, *Mater. Chem. Phys.*, 2011, **129**, 68–76.
35 A. K. Singh and M. A. Quraishi, *Corros. Sci.*, 2011, **53**, 1288–1297.
36 A. K. Singh and M. A. Quraishi, *J. Appl. Electroch.em*, 2011, **41**, 7–18.
37 S. Keera and M. Deyab, *Colloids Surf., A*, 2005, **266**, 129.
38 A. M. Hassan and T. M. H. Abdel-Fatah, *Int. J. Electrochem. Sci.*, 2016, **11**, 6959–6975.
39 S. Abd El Rehim, H. Hassan and M. Amin, *Mater. Chem. Phys.*, 2002, **78**, 337.
40 B. Hammouti, A. Dafali, R. Touzani and M. Bouachrine, *J. Saudi Chem. Soc.*, 2012, **16**, 413–418.
41 A. Amin, *Corros. Sci.*, 2004, **46**, 5–25.
42 G. Mu, X. Li and G. Liu, *Corros. Sci.*, 2005, **47**, 1932–1952.
43 A. S. Fouda, G. El-Ewady and A. H. Ali, *Green Chem. Lett. Rev.*, 2017, **10**(2), 88–100.
44 F. Mohsenifar, H. Jafari and K. Sayin, *Journal of Bio- and Tribo-Corrosion*, 2016, **2**(1), 1–13.
45 H. Jafari, K. Akbarzade and I. Danaee, *Arabian J. Chem.*, 2014, 1–8.
46 J. M. Thomas and W. J. Thomas, *Introduction to the Principles of Heterogeneous Catalysis*, Academic Press, London, 5th edn, 1981, p. 14.
47 M. I. Awad, *J. Ap. Electrochem.em*, 2006, **36**, 1163–1168.
48 N. O. Obi-Egbedi, K. E. Essien, I. B. Obot and E. E. Ebenso, *Int. J. Electrochem. Sci.*, 2011, **6**, 913–930.
49 M. M. EL-Naggar, *J. Mater. Sci.*, 2000, **35**, 6189–6195.
50 S. L. Chi-Ucán, A. Castillo-Atoche, P. C. Borges, J. A. Manzanilla-Cano, G. González-García, R. Patiño and L. Díaz-Ballote, *J. Chem.*, 2014, **2014**, 1–10.
51 H. A. Sing, E. E. Ebenso and M. A. Quraishi, *Int. J. Electrochem. Sci.*, 2012, **7**, 3409–3419.
52 P. Bothi Raja and M. G. Sethuraman, *Mater. Lett.*, 2008, **62**, 1602–1604.
53 Y. Yan, W. Li, L. Cai and B. Hou, *Electrochim. Acta*, 2008, **53**, 5953–5960.
54 E. M. Sherif, R. M. Erasmus and J. D. Collins, *J. Appl. Electrochem.*, 2009, **39**, 83–91.
55 A. M. Alfantazi, T. M. Ahmed and D. Tromans, *Mater. Des.*, 2009, **30**, 2425–2430.
56 H. Ashassi-Sorkhabi, M. R. Majidi and K. Seyyedi, *Appl. Surf. Sci.*, 2004, **225**, 176–185.
57 S. Mo, T. Ting Qin, H. Qun Luo and N. B. Li, *RSC Adv.*, 2015, **5**, 90542–90549.
58 D. A. Lopez, S. N. Simison and S. R. de Sanchez, *Electrochim. Acta*, 2003, **48**, 845–854.
59 Z. Lukacs, *J. Electroanal. Chem.*, 1999, **464**, 68–75.
60 A. S. Fouda, A. A. Ibrahim and W. T. El- behairy, *Der Pharma Chemica*, 2014, **6**(5), 144–157.
61 A. S. Fouda, A. E. Mohamed and M. A. Khalid, *J. Chem. Pharm. Res.*, 2016, **8**(2), 86–98.
62 M. El Achouri, S. Kertit, H. M. Gouttaya, B. Nciri, Y. Bensouda, L. Perez, M. R. Infante and K. Elkacemi, *Prog. Org. Coat.*, 2001, **43**, 267–273.
63 L. R. Chauhan and G. Gunasekaran, *J. Corros. Sci. Eng.*, 2007, **49**, 1143–1161.
64 K. R. Ansari, M. A. Quraishi and A. Singh, *Corros. Sci.*, 2014, **79**, 5–15.
65 M. A. Hegazy, S. S. Abd El Rehim, A. M. Badawia and M. Y. Ahmed, *RSC Adv.*, 2015, **5**, 49070–49079.
66 G. Trabanelli, C. Montecelli, V. Grassi and A. J. Frignani, *Cem. Concr. Res.*, 2005, **35**(9), 1804–1813.
67 E. Barsoukov and J. R. Macdonald, *Impedance Spectroscopy, Theory, Experiment and Applications*, Wiley Interscience publications, New York, 2nd edn, 2005.
68 M. N. El-Haddad, *RSC Adv.*, 2016, **6**, 57844–57853.
69 M. N. EL-Haddad and A. S. Fouda, *Chem. Eng. Commun.*, 2013, **200**, 1366–1393.
70 R. W. Bosch, W. F. Bogaerts and B. Syrett, *Proc. 8th International Symposium on Electrochemical Methods in Corrosion Research modulation (EFM) technique*, Nieuwpoort, Belgium, 4–9 May 2003.
71 R. W. Bosch, J. Hubrecht, W. F. Bogaerts and B. C. Syrett, *Corrosion*, 2011, **57**, 60–70.
72 N. O. Obi-Egbedia and I. B. Obotb, *Arabian J. Chem.*, 2013, **6**, 211–223.
73 J. Jeyasundari, S. Rajendran, R. S. Kannan and Y. B. A. Jacob, *Eur. Chem. Bull.*, 2013, **2**(9), 585–591.

